PROCEEDINGS OF SPIE

SPIEDigitalLibrary.org/conference-proceedings-of-spie

Tellurium doped a-Se devices for improved optical absorption in indirect x-ray photodetection

Kaitlin Hellier, Emmie Benard, Shiva Abbaszadeh

Kaitlin Hellier, Emmie Benard, Shiva Abbaszadeh, "Tellurium doped a-Se devices for improved optical absorption in indirect x-ray photodetection," Proc. SPIE 12031, Medical Imaging 2022: Physics of Medical Imaging, 120310H (4 April 2022); doi: 10.1117/12.2613150

SPIE.

Event: SPIE Medical Imaging, 2022, San Diego, California, United States

Downloaded From: https://www.spiedigitallibrary.org/conference-proceedings-of-spie on 21 Feb 2023 Terms of Use: https://www.spiedigitallibrary.org/terms-of-use

Tellurium doped a-Se devices for improved optical absorption in indirect X-ray photodetection

Kaitlin Hellier[a], Emmie Benard[b], Shiva Abbaszadeh[a*]
[a]Electrical and Computer Engineering, University of California, Santa Cruz, 1156 High St., Santa Cruz, CA, USA, 95064; [b]Arizona State University, 975 S. Myrtle Ave., Tempe, AZ, 85281

ABSTRACT

Amorphous selenium (a-Se) is a high gain, low dark current, large area compatible photoconductor that has received significant attention towards the development of UV and X-ray detectors for medical imaging. Indirect detectors utilizing a-Se often feature blue emitting scintillators due to the high attenuation coefficient of a-Se in that region. However, emission tails from the scintillators often fall out of the conversion range of a-Se, and scintillators with emission peaks outside the absorption of Se cannot be utilized. In order to improve the sensitivity and gain in a-Se indirect detectors, we propose doping a-Se with tellurium as a function of depth, where tail emission will be absorbed by the lower bandgap a-Se/Te after primary absorption in the initial Se layer. In addition, we employ a lateral device structure to avoid any absorption at short wavelengths from a transparent electrode or blocking layer. In this work, we present the first steps towards fabricating these devices. Studies of charge transport in doped a-Se/Te devices are performed using the transient photocurrent time-of-flight technique. We report hole and electron mobilities for a-$Se_{1-x}Te_x$ (x = 0, 0.01, 0.05, 0.10) as a function of applied voltage, along with band gaps and comparisons to previous studies. Fabrication of lateral devices, with and without optical slits, is demonstrated and discussed.

Keywords: amorphous selenium, selenium photoconductors, selenium-tellurium, selenium indirect detectors, selenium doping, lateral device, X-ray detection, time of fight

1. INTRODUCTION

Amorphous selenium (a-Se) is a chalcogenide glass with a bandgap of 1.9-2.2 eV that is large-area compatible, low cost, and exhibits a low dark current. Its fabrication is a mature technology and has been utilized as a direct-conversion photoconductive layer in digital flat panel detectors for mammography.[1] It is capable of avalanche multiplication at relatively low fields compared to other common avalanche materials, such as amorphous silicon.[2] These characteristics have motivated research and development of novel a-Se based detectors for different applications in life sciences, biomedical imaging, X-ray imaging, high energy physics, and industrial imaging.[3] Indirect detectors with high light yield scintillators are commonly used in commercial flat panel detectors and are easily scaled for large area detection. Several scintillator materials, such as CsI:Na and NaI:Tl, have peak emission in blue wavelengths, an ideal match for the attenuation coefficient of a-Se. Unfortunately, the emission peak and tail of many scintillator materials, like CsI: Tl, expand beyond primary a-Se absorption, lowering the optical quantum efficiency of the detector or preventing use with a-Se.[4]

Our goal is to enable detection of photons with spectral coverage from UV to red wavelengths, encompassing the entire emission spectra of UV and blue scintillators and improving indirect a-Se detector efficiencies. Doping a-Se with Te has been shown to decrease the bandgap of the material, demonstrated in Figure 1, however absorption sensitivity and charge transport suffer.[5–12] Previous works have employed thin layers of Te-doped a-Se in HARP structures to improve green to red absorbance, however experience increased dark currents and ghosting.[13,14] In order to optimize photon

*sabbasza@ucsc.com; ril.soe.ucsc.edu

Medical Imaging 2022: Physics of Medical Imaging, edited by Wei Zhao, Lifeng Yu, Proc. of SPIE
Vol. 12031, 120310H · © 2022 SPIE · 1605-7422 · doi: 10.1117/12.2613150

Downloaded From: https://www.spiedigitallibrary.org/conference-proceedings-of-spie on 21 Feb 2023
Terms of Use: https://www.spiedigitallibrary.org/terms-of-use

collection while utilizing the higher charge transport of stabilized a-Se, we will dope the a-Se layer as a function of depth. Photons will initially be absorbed and converted by the higher band-gap a-Se layer; subsequent layers, each increasing in Te content – and therefore decreasing bandgap – will absorb the remaining lower-energy photons. The Te doped layer thickness (60-120 nm) and concentration (0-30 wt. %) will be optimized to maintain low dark currents and minimize the number of trapped electrons in the doped Te layer.[15,16]

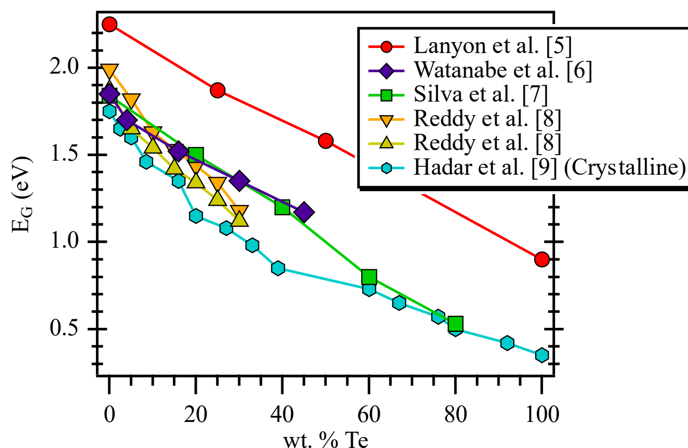

Figure 1. Reported values of band gap for Se:Te alloys from previously published studies. The two sets of values by Reddy et al. arise from two methods for fitting to absorbance spectra.[8]

Most of the research in a-Se is geared towards medical imaging, thicker device layers, and vertical device structures.[17–20] In a vertical structure the electric field is more uniform within the thickness of a-Se; however, there is a top contact and blocking layer that can undesirably absorb short-wavelength light before it reaches the photodetector. In a lateral architecture, a-Se is the top layer and there is no top contact, allowing for more direct absorption of incident photons. By utilizing a lateral structure for our a-Se/Te devices, we can further improve the short wavelength photon absorption in the device.

In this work, we will present our first steps in developing layered a-Se/Te lateral devices, in which we fabricate vertical devices with 0-10 wt. % Te dopant. We utilize a transient photocurrent time of flight (TOF) apparatus to characterize the fabricated devices and compare their performance with a previously published studies. In addition, we demonstrate the fabrication of lateral devices with and without optical slits.

2. METHODS

Transient photocurrent time of flight (TOF) is a method for characterizing the transport properties of low mobility materials, where the transit time of charge carriers across the detector is observed and used to calculate the mobility. In vertical devices, depicted in Figure 1 a), the absorption depth of the material is shorter than the thickness of the device, allowing for quick collection of one polarity of charge carriers (electrons or holes) at the transparent electrode, and measurement of the transit time of the charge carriers of the other polarity by collection at the other electrode. In a lateral device, a comb structure is used to apply a field across the active material, with alternating electrode arms biased positively and negatively. In lateral devices, the entire active layer is exposed to the incident light, preventing distinction between carriers. Optical slits have been used to eliminate this issue in TOF of organic detectors.[21] By placing optical slits around one polarity, charge specific TOF can be performed. The optical slit around the electrode leads to the quick collection of the corresponding carrier, while the other drifts across the longer, unexposed region of the device, and results in the domination of that carrier in the transit time observed in the signal. By reversing the polarity of the electrodes, we can

Downloaded From: https://www.spiedigitallibrary.org/conference-proceedings-of-spie on 21 Feb 2023
Terms of Use: https://www.spiedigitallibrary.org/terms-of-use

measure the transit time of the other carrier. To understand the transport in our lateral a-Se/Te devices, we prepare vertical devices to later compare to lateral devices with optical slits, and present electron and hole mobilities for these materials.

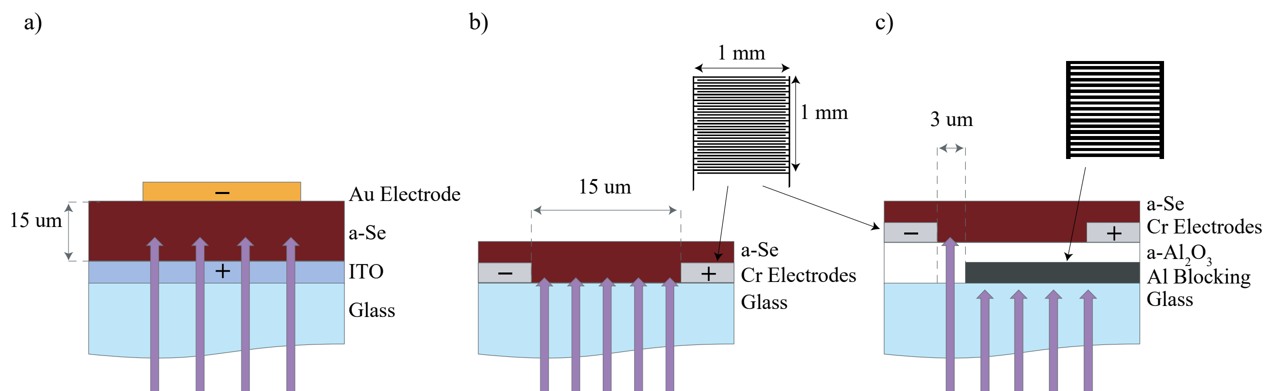

Figure 2. Schematics of the three device architectures tested in this work. a) A vertical device, b) a 1 mm by 1 mm lateral device, in which the incident light is incident upon the entire active layer, and c) a lateral device employing optical slits, in which light is blocked except around one electrode, allowing for single carrier studies.

2.1 Device Fabrication

Vertical devices were fabricated to compare extracted mobilities with those reported previously. All substrates were first cleaned by ultrasonication in acetone and isopropyl alcohol, each for 10 minutes, followed by rinsing with deionized water and drying with nitrogen. Vertical devices were prepared by the thermal evaporation of 15 um stabilized a-Se and pure Se doped with 0, 1, 5, and 10 wt. % Te [stabilized (0.2% As, 10 ppm Cl) and 10% Te from Amalgamet Canada LP, pure (99.999%) Se from Puratronic] on glass/ITO substrates (Delta Technologies, 70-100 Ohms/sq.), followed by thermal evaporation of 100 nm Au as top electrodes. A schematic of the devices is given in Figure 2 a). Lateral devices were prepared by patterning via photolithography on fused silica substrates, with and without optical slits. Devices with 3 um optical slits were patterned with a 50 nm thick Al blocking layer, depicted in Figure 2 c), which was insulated from electrodes by a 100 nm thick layer of Al_2O_3. The lateral device comb-structure was then fabricated by patterning 15 um wide Cr electrodes with 15 um separation; devices without optical slits were patterned in this way directly on glass, seen in Figure 2 b). For both devices with and without optical slits, 500 nm of a-Se/Te was deposited on top of the electrodes. Additional 500 nm films were deposited on fused silica for optical measurements.

2.2 X-ray Diffraction and Transmission

X-ray diffraction was performed on a Rigaku Miniflex II Powder Diffractometer at a voltage of 30 kV and current of 15 mA, and scanning angle from 10-70° with a step size of 0.02° at 3°/min. UV-visible transmission measurements were performed on a Jasco V670 spectrophotometer from 200-900 nm with background subtraction of the fused silica substrate. Transmission data was converted to absorbance by Beer-Lambert's law, $A = -\log(T)$; from this, Tauc fits were performed assuming an indirect transition, where $\alpha h\nu \propto (h\nu - E_g)^2$, and the band gap was extracted.

2.3 Time of flight characterization

Time of flight (TOF) was performed on vertical devices to determine the mobility of charge carriers in the a-Se/Te. A schematic of the TOF system is shown in Figure 3. A pulsed 355 nm DPSS laser (EKSPLA), with 30 uJ maximum intensity and a pulse width of 25 ps passes through a 50/50 UV fused silica beam splitter (Thorlabs), where it is split to an energy meter and to the sample. To ensure a small signal condition, the laser is attenuated by both power settings and neutral density filters. Devices are biased from 5-30 V/um using a high voltage source. The signal generated is read out on a high precision Tektronix oscilloscope with 50 Ohm impedance. All electronic components are kept at matching impedance to prevent any reflections. The laser is incident upon vertical devices parallel to the applied field; it is incident upon the lateral devices perpendicular to the applied field.

Downloaded From: https://www.spiedigitallibrary.org/conference-proceedings-of-spie on 21 Feb 2023
Terms of Use: https://www.spiedigitallibrary.org/terms-of-use

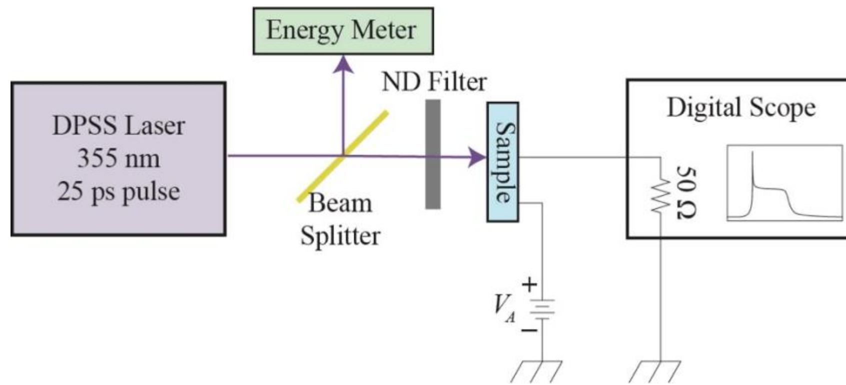

Figure 3. A schematic of the time of flight (TOF) setup employed in this work.

Mobility, μ, is extracted from the TOF signal by calculating the charge transit time, t_T, between the onset of charge collection and the point at which lines fit to the plateau and tail intersect. Figure 4 gives an example of a typical TOF signal and the fits used to determine the transit time. Combining this with the known thickness, L, and applied voltage, V_A, we have

$$\mu = \frac{L^2}{V_A t_T} . \tag{1}$$

The ITO electrode in a vertical device can be biased positively or negatively, allowing for hole and electron mobilities to extracted, respectively.

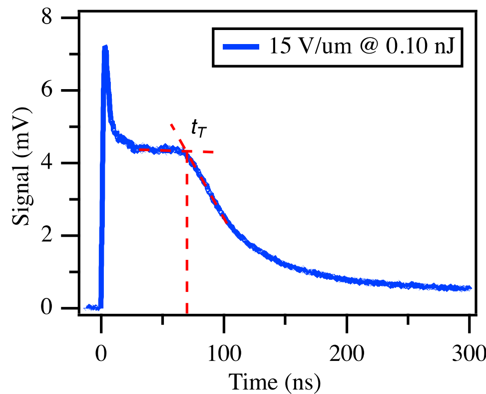

Figure 4. Example of TOF signal performed on a 15 um vertical a-Se (0.2% As, 10 ppm Cl) device. The ITO was biased at +225 V, with a laser intensity of 1.0 uJ and an ND4 filter (0.01% transmission) in place.

3. RESULTS & DISCUSSION

X-ray diffraction was performed on stabilized Se and 10 wt. % Te samples to ensure samples were amorphous; it is commonly noted that crystallization may occur at concentrations of 30% or higher.[5,6] Both samples exhibit amorphous behavior, shown in Figure 5 a), with no sharp peaks and a broad, low intensity peak from 10-38°, common in amorphous and glassy materials.

Downloaded From: https://www.spiedigitallibrary.org/conference-proceedings-of-spie on 21 Feb 2023
Terms of Use: https://www.spiedigitallibrary.org/terms-of-use

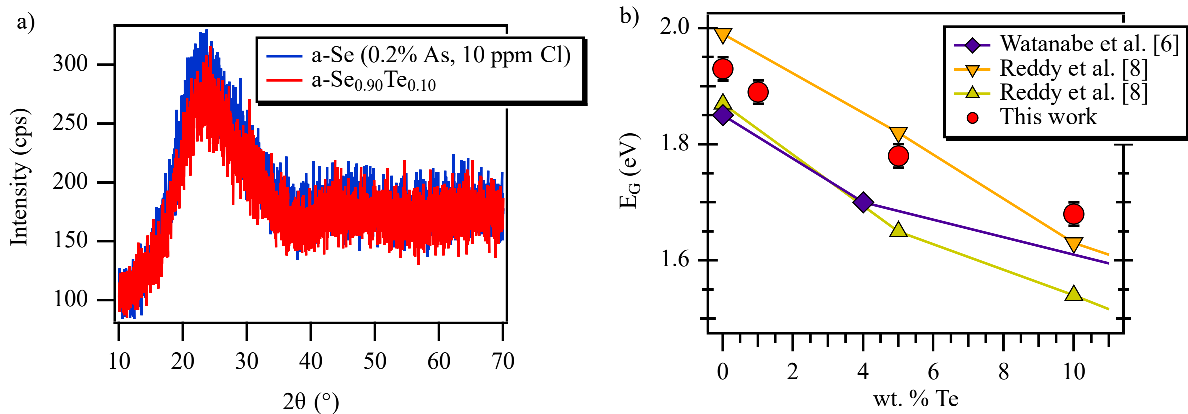

Figure 5. a) X-ray diffraction of stabilized Se and a-$Se_{0.9}Te_{0.1}$, showing an amorphous structure. b) Comparison of the extracted band gaps as a function of Te doping in this work (red circles) with those reported in selected works. The two fit methods used by Reddy et al. demonstrate the variance that can be observed based on the technique used for calculating band gap values.

Extracted band gaps for each sample are given in Figure 5 b), alongside selected works from Figure 1. A reduction in band gap energy is observed with increasing Te content, as expected. Values extracted are also in line with previous reports, within error due to instrumentation and the band gap extraction technique used.

Transient photocurrent TOF measurements of a-$Se_{1-x}Te_x$vertical devices were performed for devices with x = 0, 0.1, 0.5, and 0.10 from 5-30 V/um. The extracted hole and electron mobilities can be found in Figure 6 a) and b), respectively. It can be seen that even the slightest inclusion of Te results in a drastic reduction in mobility for both carriers – stronger for holes, though still significant for electrons - and even further reductions for increasing values of Te. Despite this drop, both hole and electron mobilities increase with increasing field, much like stabilized Se.

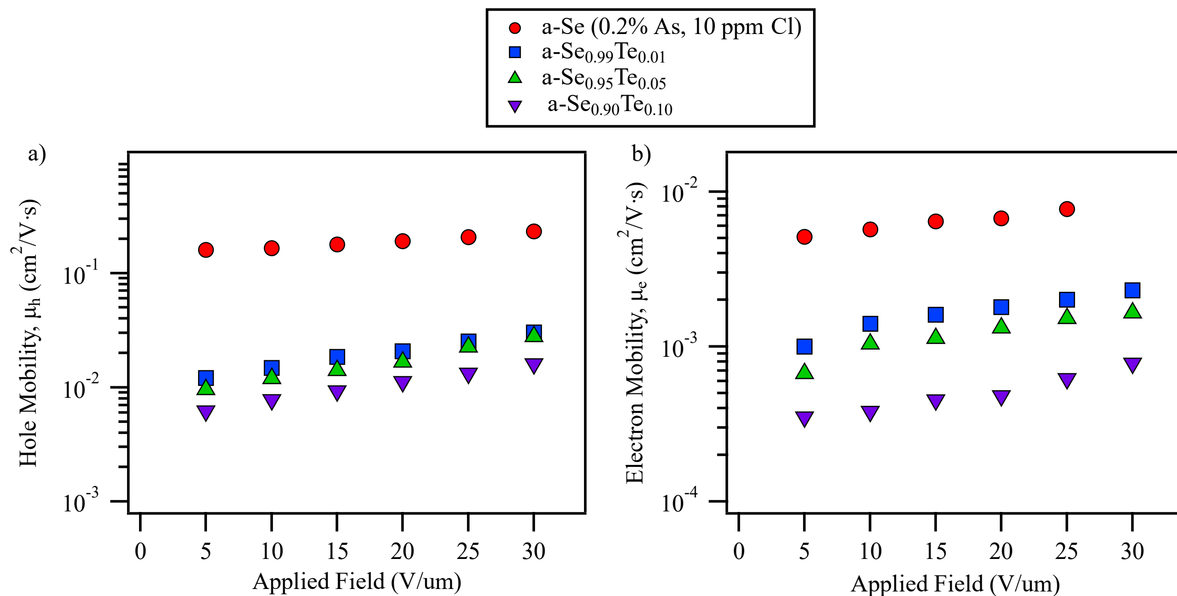

Figure 6. Mobilities for a) holes and b) electrons for a-$Se_{1-x}Te_x$, x = 0, 0.1, 0.5, and 0.10, with applied field ranging from 5-30 V/um. The laser intensity was adjusted and kept as low as possible for all measurements.

Downloaded From: https://www.spiedigitallibrary.org/conference-proceedings-of-spie on 21 Feb 2023
Terms of Use: https://www.spiedigitallibrary.org/terms-of-use

Figure 7 compares the results of this work with those reported by Kasap and Juhasz. The mobilities reported in this work are comparable with previously reported studies, with additional electron mobilities reported for the higher Te concentrations.[11,12] The mobility of the a-$Se_{0.99}Te_{0.01}$ sample is lower than what might be extrapolated from Kasap's work, indicating that, though the mixture of Se:Te prior to evaporation should have resulted in 1% Te, the deposited composition may vary from the intended value. Further studies on the resulting compositions would be of benefit for small, precise doping levels to ensure optimal selection for lateral devices.

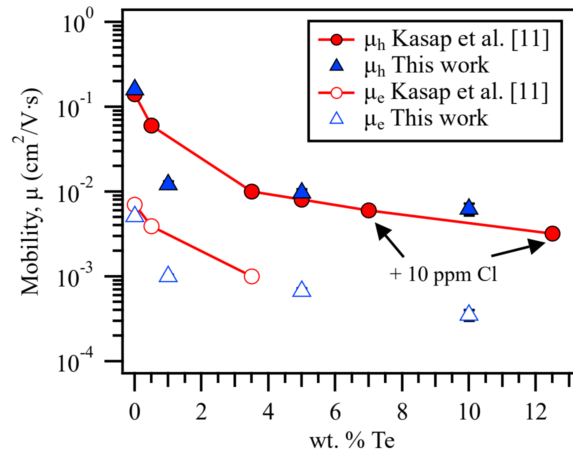

Figure 7. Comparison of the hole and electron mobilities from this work with those reported by Kasap and Juhasz at an applied field of 5 V/um. Note that the mobility shown for Kasap's 7 and 12.5 wt. % Te includes 10 ppm Cl, as they did not report for those concentrations without Cl dopants. They also did not observe electron mobilities for concentrations greater than 3%.

It should also be noted that Kasap and Juhasz explored the effect of doping a-Se/Te with Cl, similar to what is commonly done in stabilized Se, to mitigate deep defects and improve transport. Several studies have come to the conclusion that Te doping results in several new deep and shallow defect states.[12,22,23] The incorporation of small levels of chlorine is able to mitigate deep trap states, however results in even more shallow traps, further reducing mobility despite increasing carrier lifetimes.[11,24]

Lateral devices, both with and without optical slits, have been fabricated with stabilized a-Se and a-$Se_{0.9}Te_{0.1}$, as seen in Figure 8. Modifications to the existing TOF setup, including those previously mentioned, are in progress to allow testing of the devices, which follow a differing architectural design, and therefore testing setup, from the vertical devices.

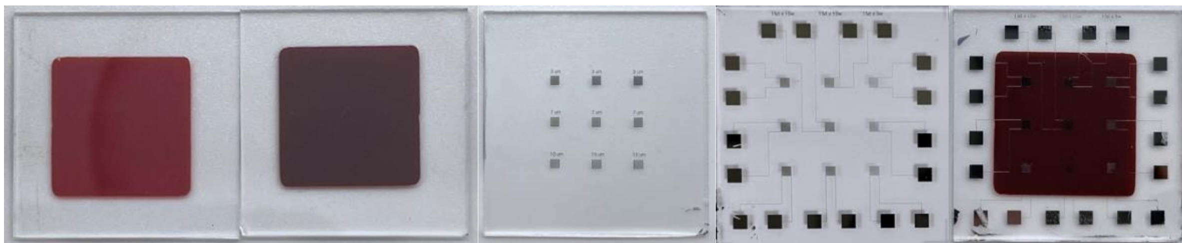

Figure 8. From left to right: 500 nm films of stabilized a-Se and a-$Se_{0.9}Te_{0.1}$, optical slit blocking layer, lateral device electrodes, and a completed a-$Se_{0.9}Te_{0.1}$ lateral device with optical slits.

Downloaded From: https://www.spiedigitallibrary.org/conference-proceedings-of-spie on 21 Feb 2023
Terms of Use: https://www.spiedigitallibrary.org/terms-of-use

4. CONCLUSIONS

We have reported hole and electron mobilities for a-$Se_{1-x}Te_x$ (x = 0, 0.01, 0.05, 0.10) vertical devices, along with band gaps for each concentration. The observed band gap decreases with increasing inclusion of Te and follows trends from previous works. Mobilities are also in line with previous studies, demonstrating proper characterization technique, fabrication, and reproducibility. Mobility as a function of applied electric field is given up to 30 V/um, not previously reported. Lateral devices utilizing optical slits have been fabricated, preparing the way for transient photocurrent time of flight measurements and mobility extraction for a different architecture. This work presents the first stages in the development of lateral detectors comprised of a-Se doped with Te as a function of depth, which will allow for improved photon collection and efficiency in indirect detection for medical imaging.

ACKNOWLEDGEMENTS

Funding for this work was provide in part by DOE grant number DE-SC0021975 and from Western Digital Corporation. We acknowledge Jeremy Barnett and the X-ray Facility at University of California Santa Cruz for use of the Rigaku Miniflex Diffractometer, funded by NSF MRI grant number 1126845, and or assistance with X-ray diffraction. We also acknowledge Roy Sfadia and the Thin-Film Optoelectronics Laboratory for their assistance in taking UV-visible transmission measurements.

REFERENCES

[1] Kasap, S., Frey, J. B., Belev, G., Tousignant, O., Mani, H., Laperriere, L., Reznik, A. and Rowlands, J. A., "Amorphous selenium and its alloys from early xeroradiography to high resolution X-ray image detectors and ultrasensitive imaging tubes," Phys. Status Solidi B **246**(8), 1794–1805 (2009).

[2] Reznik, A., Baranovskii, S. D., Rubel, O., Juska, G., Kasap, S. O., Ohkawa, Y., Tanioka, K. and Rowlands, J. A., "Avalanche multiplication phenomenon in amorphous semiconductors: Amorphous selenium versus hydrogenated amorphous silicon," J. Appl. Phys. **102**(5), 053711 (2007).

[3] Huang, H. and Abbaszadeh, S., "Recent Developments of Amorphous Selenium-Based X-Ray Detectors: A Review," IEEE Sens. J. **20**(4), 1694–1704 (2020).

[4] Wang, K. and Karim, K., [Lateral Amorphous Selenium Detector for Large Area, High Speed, and High Energy X-ray Imaging] (2010).

[5] Lanyon, H. P. D., "Optical and Electrical Properties of Selenium-Tellurium Alloys," J. Appl. Phys. **35**, 1516–1523 (1964).

[6] Watanabe, H. and Kao, K. C., "Structure and Properties of $Se_{1-x}Te_x$ Films," Jpn. J. Appl. Phys. **18**(9), 1849–1850 (1979).

[7] Silva, L. A. and Cutler, M., "Optical properties of liquid Se-Te alloys," Phys. Rev. B **42**(11), 7103–7113 (1990).

[8] Reddy, K. V. and Bhatnagar, A. K., "Electrical and optical studies on amorphous Se-Te alloys," J. Phys. Appl. Phys. **25**(12), 1810–1816 (1992).

[9] Hadar, I., Hu, X., Luo, Z.-Z., Dravid, V. P. and Kanatzidis, M. G., "Nonlinear Band Gap Tunability in Selenium–Tellurium Alloys and Its Utilization in Solar Cells," ACS Energy Lett. **4**(9), 2137–2143 (2019).

[10] Park, W.-D. and Tanioka, K., "Spectral Responses of Te-Doped a-Se High-Gain Avalanche Rushing Amorphous Photoconductor (HARP) Films for a Solid State Image Sensor," Jpn. J. Appl. Phys. **42**(4S), 1954 (2003).

[11] Kasap, S. O. and Juhasz, C., "Charge transport in chlorine doped amorphous Se:Te xerographic photoreceptor films," J. Non-Cryst. Solids **72**(1), 23–37 (1985).

[12] Juhasz, C., Vaezi-Nejad, M. and Kasap, S. O., "Xerographic properties of single- and double-layer photoreceptors based on amorphous selenium-tellurium alloys," J. Mater. Sci. **22**(7), 2569–2582 (1987).

[13] Park, W.-D. and Tanioka, K., "Dependence of Thickness on Avalanche Characteristics of Te-Doped Amorphous Selenium Photoconductive Target," Jpn. J. Appl. Phys. **48**(4S), 04C159 (2009).

[14] Orlik, C., Howansky, A. F., Léveillé, S., Mishchenko, A., Kasap, S., Stavro, J., Goldan, A. H., Scheuermann, J. R. and Zhao, W., "Improved optical quantum efficiency and temporal performance of a flat-panel imager with avalanche gain," Med. Imaging 2021 Phys. Med. Imaging **11595**, 313–320, SPIE (2021).

[15] Matsubara, T., Ohkawa, Y., Miyakawa, K., Suzuki, S., Kubota, M., Egami, N., Tanioka, K., Ogusu, K., Kobayashi, A., Hirai, T. and Kawai, T., "Improvement in photoelectric conversion efficiency of red light in

Downloaded From: https://www.spiedigitallibrary.org/conference-proceedings-of-spie on 21 Feb 2023
Terms of Use: https://www.spiedigitallibrary.org/terms-of-use

HARP film," Sens. Cameras Syst. Sci. Appl. VIII **6501**, 650108, International Society for Optics and Photonics (2007).

[16] Ohkawa, Y., Miyakawa, K., Matsubara, T., Kikuchi, K., Suzuki, S., Tanioka, K., Kubota, M., Egami, N. and Kobayashi, A., "Heat treatment to suppress image defect occurrence in amorphous selenium avalanche multiplication photoconductive film with improved red-light sensitivity," IEICE Electron Express (2009).

[17] Goldan, A. H. and Zhao, W., "A field-shaping multi-well avalanche detector for direct conversion amorphous selenium," Med. Phys. **40**(1), 010702 (2013).

[18] Arnab, S. M. and Kabir, M. Z., "Impact of Lubberts Effect on Amorphous Selenium Indirect Conversion Avalanche Detector for Medical X-Ray Imaging," IEEE Trans. Radiat. Plasma Med. Sci. **1**(3), 221–228 (2017).

[19] Stavro, J., Goldan, A. H. and Zhao, W., "Photon counting performance of amorphous selenium and its dependence on detector structure," Med. Imaging 2018 Phys. Med. Imaging **10573**, 105735Y, International Society for Optics and Photonics (2018).

[20] LaBella, A., Stavro, J., Léveillé, S., Zhao, W. and Goldan, A. H., "Picosecond Time Resolution with Avalanche Amorphous Selenium," ACS Photonics **6**(6), 1338–1344 (2019).

[21] Kuwahara, A., Naka, S., Okada, H. and Onnagawa, H., "Carrier mobility of organic thin films using lateral electrode structure with optical slits," Appl. Phys. Lett. **89**(13), 132106 (2006).

[22] Perron, J. C., "Electrical and thermoelectrical properties of selenium-tellurium liquid alloys," Adv. Phys. **16**(64), 657–666 (1967).

[23] Takahashi, T., "Drift mobilities in amorphous As-Se-Te," J. Non-Cryst. Solids **34**(3), 307–312 (1979).

[24] Polischuk, B., Kasap, S. O., Aiyah, V., Scansen, D. and Bekirov, A., "Charge carrier trapping in chalcogenide semiconductors," J. Non-Cryst. Solids **137–138**, 943–946 (1991).

Downloaded From: https://www.spiedigitallibrary.org/conference-proceedings-of-spie on 21 Feb 2023
Terms of Use: https://www.spiedigitallibrary.org/terms-of-use